Vol 461|10 September 2009|doi:10.1038/nature08288

LETTERS

Stable single-unit-cell nanosheets of zeolite MFI as active and long-lived catalysts

Minkee Choi[1]*, Kyungsu Na[1]*, Jeongnam Kim[1,2], Yasuhiro Sakamoto[5,6], Osamu Terasaki[4,6] & Ryong Ryoo[1,2,3]

Zeolites—microporous crystalline aluminosilicates—are widely used in petrochemistry and fine-chemical synthesis[1–3] because strong acid sites within their uniform micropores enable size- and shape-selective catalysis. But the very presence of the micropores, with aperture diameters below 1 nm, often goes hand-in-hand with diffusion limitations[3–5] that adversely affect catalytic activity. The problem can be overcome by reducing the thickness of the zeolite crystals, which reduces diffusion path lengths and thus improves molecular diffusion[4,5]. This has been realized by synthesizing zeolite nanocrystals[6], by exfoliating layered zeolites[7–9], and by introducing mesopores in the microporous material through templating strategies[10–17] or demetallation processes[18–22]. But except for the exfoliation, none of these strategies has produced 'ultrathin' zeolites with thicknesses below 5 nm. Here we show that appropriately designed bifunctional surfactants can direct the formation of zeolite structures on the mesoporous and microporous length scales simultaneously and thus yield MFI (ZSM-5, one of the most important catalysts in the petrochemical industry) zeolite nanosheets that are only 2 nm thick, which corresponds to the *b*-axis dimension of a single MFI unit cell. The large number of acid sites on the external surface of these zeolites renders them highly active for the catalytic conversion of large organic molecules, and the reduced crystal thickness facilitates diffusion and thereby dramatically suppresses catalyst deactivation through coke deposition during methanol-to-gasoline conversion. We expect that our synthesis approach could be applied to other zeolites to improve their performance in a range of important catalytic applications.

In principle, zeolites will exhibit maximized molecular diffusion if the thickness of the crystal is reduced to the single unit cell dimension. Isolated zeolite unit cells (zero-dimensional crystal structure), nanowires (one-dimensional) and nanosheets (two-dimensional) would be obtained when confining the crystal thickness to the dimension of a single unit cell along three, two and one spatial dimensions, respectively. Of these three types of ultrathin zeolites, nanowires and nanosheets would be preferred in heterogeneous catalysis because of their ease of handling (they are collectable by filtration).

Although such ultrathin zeolites are easy to imagine, their actual synthesis is extremely difficult. This is because zeolite crystallization, like other crystallization processes, is accompanied by Ostwald ripening. Ostwald ripening is a naturally and spontaneously occurring process that minimizes the surface free energy of crystals, resulting in dissolution of smaller crystals and further growth of larger crystals. This thermodynamically controlled phenomenon becomes more significant as the crystal size decreases and therefore renders the synthesis of ultrathin zeolites extremely challenging. Although careful optimization of crystallization conditions[6], or use of solid templates[10–13] or organosilanes[14–16] during synthesis resulted in zeolites with significantly reduced framework thicknesses, thicknesses were typically still between 5 and 100 nm. Only the layer-by-layer exfoliation of a MWW (MCM-22) zeolite crystal[7–9] yielded zeolites with ultrathin frameworks less than 5 nm thick.

We approached the synthesis of MFI nanosheets by designing a diquaternary ammonium-type surfactant, $C_{22}H_{45}$-$N^+(CH_3)_2$-C_6H_{12}-$N^+(CH_3)_2$-C_6H_{13} (designated $C_{22\text{-}6\text{-}6}$ hereafter)[23]. The surfactant was composed of a long-chain alkyl group (C22) and two quaternary ammonium groups spaced by a C6 alkyl linkage (see Supplementary Fig. 1 for the three-dimensional molecular structure). The diammonium head group acted as an effective structure-directing agent for the MFI zeolite, while the hydrophobic interaction between the long-chain tails induced the formation of mesoscale micellar structure. With the surfactant, an ultrathin zeolite framework was formed at the hydrophilic part of the micelles while the hydrophobic tail restricted the excessive growth of zeolites. It is noteworthy that ordinary surfactants, with a single quaternary ammonium group, failed to function as an effective structure-directing agent for zeolite (generating amorphous MCM-41-type silicas)[24,25].

MFI zeolites with Si/Al ratio of 30 to ∞ were crystallized by using the diammonium surfactant as a structure-directing agent. In a typical synthesis condition (Methods), the zeolite was obtained as multilamellar stacking of MFI nanosheets that were three-dimensionally intergrown (Fig. 1a). The overall thickness of the lamellar stacking was normally 20–40 nm. High-resolution transmission electron microscope (TEM) investigation of the cross-section (Fig. 1c) revealed that the stacking was composed of alternating layers of 2.0-nm-thick MFI zeolite framework and 2.8-nm-thick surfactant micelles. The zeolite layer was composed of three pentasil sheets, which corresponded to a single unit cell dimension along the *b*-axis ($b = 1.9738$ nm). TEM investigation and electron diffraction on the layer surface identified it as the (010) surface of the MFI framework (Fig. 1b). The short arc in the electron diffraction pattern (Fig. 1b) indicated that each zeolite layer possessed high structural correlation in the *a*–*c* plane orientation with a minor deviation. Only the *h*0*l* reflections were sufficiently sharp for indexing in the powder X-ray diffraction pattern (Fig. 1d), confirming that the zeolite layer possessed large coherent domains characterized by wide *a*–*c* planes while the framework thickness along the *b*-axis was extremely small. Elemental analysis revealed that the surfactant content was about 45 wt% of the as-synthesized product. The surfactant content could be decreased to 19 wt% (that is, a SiO_2/surfactant molar ratio of 37) by extraction with an HCl/ethanol solution. The non-extractable content is supposed to be the amount entrapped in the zeolite micropores after the surfactant has acted as a structure-directing agent. The extractable portion is attributed to the surfactant molecules that are located in the surfactant micelle as 'dummy' filler. On the basis of the elemental analysis and

[1]Center for Functional Nanomaterials, Department of Chemistry, KAIST, [2]Graduate School of Nanoscience and Technology (WCU), KAIST, [3]KAIST Institute for the NanoCentury, [4]Graduate School of EEWS (WCU), KAIST, Daejeon 305-701, Korea. [5]Structural Chemistry, Arrhenius Laboratory, Stockholm University, 10691 Stockholm, Sweden. [6]Nanoscience and Nanotechnology Research Center, Osaka Prefecture University, Sakai 599-8570, Japan.
*These authors contributed equally to this work.

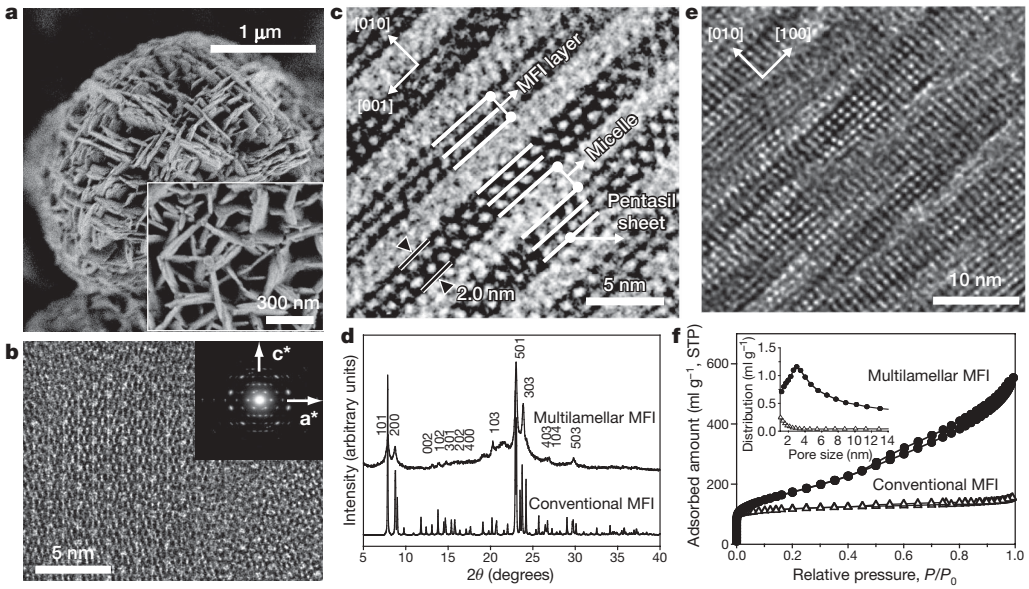

Figure 1 | MFI nanosheets with a multilamellar structure. **a**–**d**, As-synthesized sample; **e** and **f**, calcined sample. **a**, SEM image showing that the MFI zeolite has a plate-like morphology that is composed of three-dimensionally intergrown nanosheets. **b**, TEM and electron diffraction on the wide plane of the plate ([010] incidence of MFI). **c**, TEM cross-section of the plate revealing that the each plate is composed of lamellar stacking of alternating layers of MFI (2 nm) and surfactant micelle (2.8 nm). The MFI layer is composed of three pentasil sheets, corresponding to the thickness of a single unit cell dimension along the *b*-axis of $b = 1.9738$ nm. **d**, Powder X-ray diffraction pattern indicating that only *h*0*l* reflections are sufficiently sharp for indexing. The result confirms that the zeolite possesses wide *a*–*c* planes having large coherent domains, while the framework thickness along the *b*-axis is extremely small. **e**, TEM image of calcined sample showing that calcination leads to partial condensation between MFI layers, while the interlayer space (mesoporosity) is still mainly intact. **f**, N_2 adsorption–desorption isotherm, also confirming the highly mesoporous structure of the calcined sample. BET area = 520 $m^2 g^{-1}$. STP, standard temperature and pressure.

aforementioned TEM investigations, we propose that the material is composed of MFI layers wherein the surfactant molecules are aligned along the straight micropores of the MFI framework (Fig. 2a).

Because the surfactant layers provide interlamellar support (Fig. 2b), surfactant removal was expected to lead to the complete condensation of the MFI layers. However, the calcination actually led to a partial condensation only (Fig. 1e). The calcined product was highly mesoporous, although the mesopore size distribution was rather broad owing to the irregular distortion of zeolite layers (Fig. 1f). The calcined sample still exhibited a markedly enhanced Brunauer–Emmett–Teller (BET) area (520 $m^2 g^{-1}$) compared to conventional MFI zeolite (420 $m^2 g^{-1}$). The retained mesoporosity can be explained as follows. First, as indicated by the scanning electron microscope (SEM) image (Fig. 1a), there were a large number of crystal intergrowths. The intergrown crystals could act as a 'pillar' supporting each other, preventing complete collapse of the mesoporous structure. Second, there were

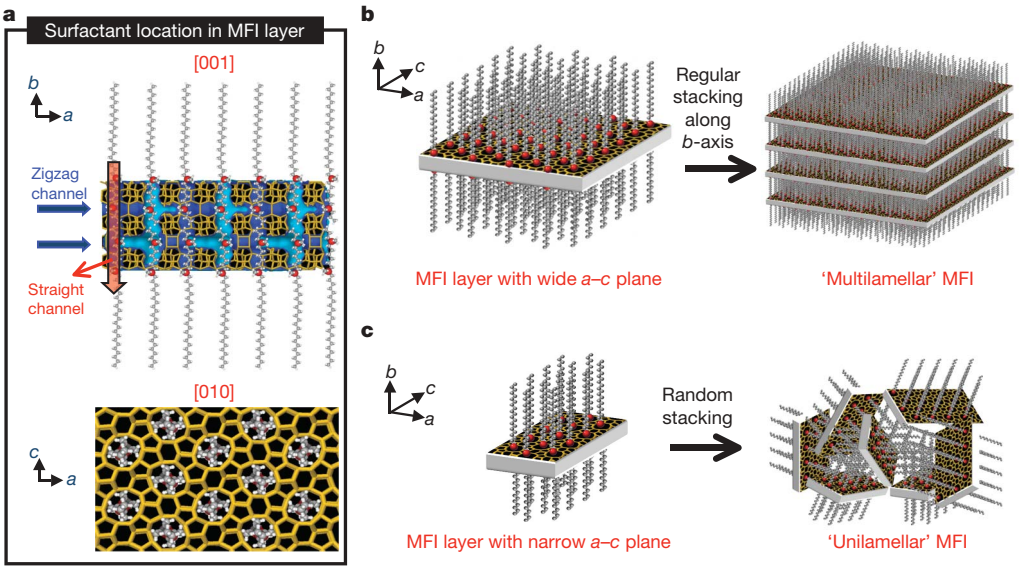

Figure 2 | Crystallization of MFI nanosheets. **a**, Proposed structure model for the single MFI nanosheet. Surfactant molecules are aligned along the straight channel of MFI framework. Two quaternary ammonium groups (indicated as a red sphere) are located at the channel intersections; one is inside the framework, and the other is at the pore mouth of the external surface. Many MFI nanosheets form either multilamellar stacking along the *b*-axis (**b**), or a random assembly of unilamellar structure (**c**).

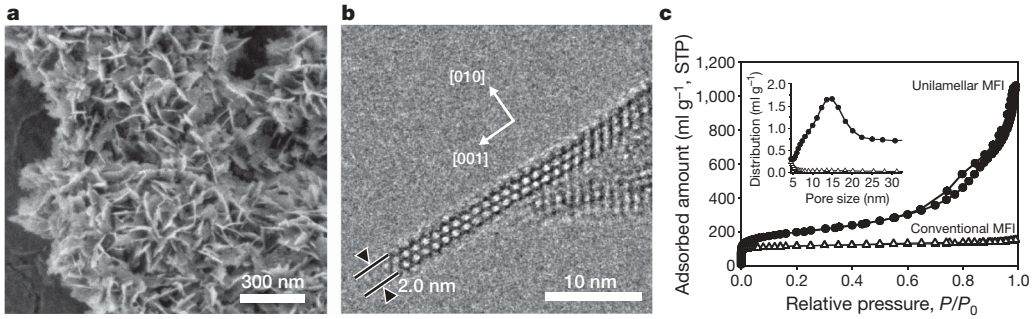

Figure 3 | MFI nanosheets with a unilamellar structure. a, SEM image showing that the MFI zeolite is synthesized in a flake-like morphology. **b**, TEM image of the cross-section of the flake, revealing that each flake is composed of a discrete MFI layer having unit cell thickness along the *b*-axis of $b = 1.9738$ nm. **c**, N_2 adsorption–desorption isotherm confirming the highly mesoporous structure of the calcined sample. BET area = 710 $m^2 g^{-1}$.

slight deviations of the crystal orientation in the *a*–*c* plane, and this mismatch between the position of silanol groups on each MFI layers prevented the complete condensation of MFI layers.

In addition to the multilamellar form, MFI zeolite could also be synthesized in the form of unilamellar nanosheets (Fig. 3a) by reducing the concentration of Na^+ in the synthesis mixture (Methods). TEM images (Fig. 3b) revealed that the material was composed of a single MFI layer (that is, three pentasil sheets) having a very narrow *a*–*c* plane; this material can thus be considered to be composed of essentially the same building blocks as the multilamellar form but without long-range stacking along the *b*-axis (Fig. 2c). The ability to produce these different forms indicates that crystal growth in the *a*–*c* plane and layer stacking along the *b*-axis are significantly affected by the concentration of Na^+ in the synthesis mixture. The unilamellar zeolite exhibited a significantly increased surface area (710 $m^2 g^{-1}$), compared to its multilamellar counterpart (520 $m^2 g^{-1}$) (Fig. 3c).

The catalytic performance of the MFI nanosheets was investigated using large organic molecules so that diffusion of the reactant molecules constrains the reaction (Methods)[26]. As expected, the catalytic activities (per weight of catalyst) of the MFI nanosheets were much higher than those of conventional MFI zeolite (see Table 1). These enhanced catalytic activities can be attributed to a large number of acid sites located at the mesopore surface (that is, on the external surface of the zeolite layer) of MFI nanosheets, with the unilamellar MFI generally exhibiting higher activities owing to its larger external surface area after calcination.

Another remarkable feature of the MFI nanosheets is their increased catalyst lifetime, which manifested itself when we investigated the catalytic properties of MFI zeolites in methanol-to-gasoline conversion. Owing to methanol's small size, there was no significant difference in the initial catalytic activity between the ultrathin and the conventional MFI zeolite. With time on-stream, however, the MFI nanosheets were deactivated far more slowly than the conventional MFI (Fig. 4). To determine why, we monitored the quantity and location of coke formation during the reaction (Methods). As shown in Fig. 4, the MFI nanosheets exhibited not only much slower coke deposition than the conventional MFI (45 versus 170 mg g^{-1} zeolite at 5 days), but also coke formation almost exclusively at the external surface (that is, mesopores) while the conventional MFI zeolite showed major coke formation inside the micropores. Coke deposition within micropores causes more effective catalyst deactivation than external coke formation[27,28] because internally deposited coke can cover the catalytically active acid sites and also block micropores already at low coking levels; in contrast, external coke causes relatively little hindrance to diffusion unless it covers the entire external catalyst surface. We therefore propose that the long catalytic lifetime of the MFI nanosheets is due to the slow deposition of coke exclusively at external zeolite surfaces, which arises because of facile mass transfer of coke precursors out of the zeolite micropores. Although we observed slow catalyst deactivation in the methanol-to-gasoline case study, it is expected that the MFI nanosheets would generally show high catalyst lifetime in various reactions[29].

The MFI nanosheets exhibited excellent thermal stability (Supplementary Fig. 2), hydrothermal stability (Supplementary Fig. 3) and strong acidity (Supplementary Fig. 4 and Supplementary Table 1), which are important for many catalytic applications. ^{27}Al magic-angle spinning NMR spectra indicated that approximately 50% of the initial tetrahedral Al was retained in the zeolite framework even after being heated in 100% steam at 700 °C (Supplementary Fig. 5). In initial experiments, we also used the present synthesis strategy to create nanosheets of the zeolite MTW (Supplementary Figs 6 and 7). This suggests that the structure-directing strategy that targets the mesoporous and microporous length scales simultaneously is fairly general, and that it can be extended to other zeolite structures and zeotype materials through the design of suitable bifunctional surfactants. The next challenge is to synthesize such porous materials in the form of continuous films or membranes for advanced applications in catalysis, adsorption, separation and sensor technologies.

Table 1 | Catalytic conversion of bulky molecules over MFI zeolites

Reactions	Conventional MFI (Si/Al = 41)	Multilamellar MFI nanosheets (Si/Al = 48)	Unilamellar MFI nanosheets (Si/Al = 53)
Cracking of branched polyethylene (HDPE)	27	45	85
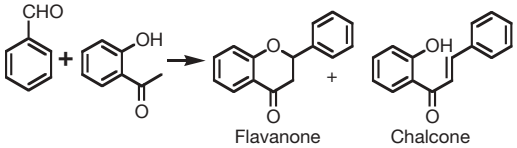 Flavanone Chalcone	16 (50/50/0)*	48 (62/28/10)*	76 (64/31/5)*
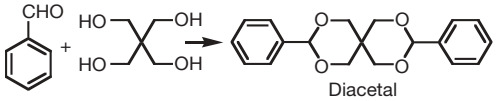 Diacetal	42	86	86

Catalytic activities were compared on the basis of the same weight of catalyst (see Methods for reaction conditions). *The numbers in parentheses indicate percentage selectivity: (flavanone/chalcone/others). All other numbers indicate the percentage reactant conversion, reproducible within 3% over three runs. HDPE, high-density polyethylene.

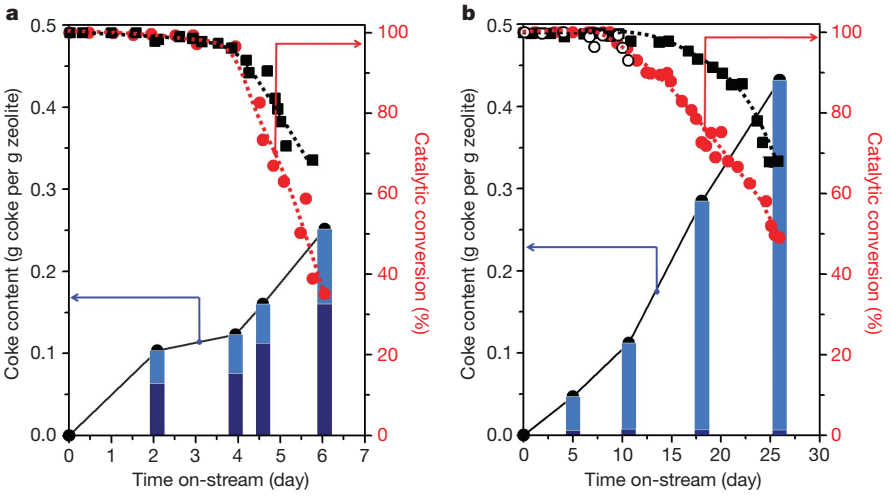

Figure 4 | Coke deposition in MFI zeolite catalysts during methanol-to-gasoline conversion. **a**, Conventional MFI zeolite. **b**, Unilamellar MFI zeolite. The unilamellar MFI zeolite exhibits a dramatically increased catalytic lifetime compared with its conventional counterpart, which is related to the preferential formation of coke in mesopores. Catalytic conversion over the unilamellar MFI was repeatedly investigated using three different synthesis batches (red circles, black squares, open circles, respectively). The catalytic measurement for conventional zeolite was repeated twice using the same sample (red circles and black squares). The solid black lines and the dotted red and black lines are guides to the eye. Dark blue bars indicate internal (inside the micropores of the zeolite) coke content, and light blue bars indicate external coke content.

METHODS SUMMARY

The $C_{22\text{-}6\text{-}6}$ surfactant was synthesized in the bromide form, that is, $C_{22\text{-}6\text{-}6}Br_2$. This surfactant was mixed with tetraethylorthosilicate (or sodium silicates), aluminium sulphate, NaOH, H_2SO_4 and distilled water, to give a molar composition of $30\,Na_2O$:$1\,Al_2O_3$:$100\,SiO_2$:$10\,C_{22\text{-}6\text{-}6}Br_2$:$18\,H_2SO_4$:$4{,}000\,H_2O$. This mixture was heated at 150 °C for 5 days in an autoclave (set on 'tumbling'), to obtain the multilamellar MFI zeolite. The unilamellar MFI zeolite was synthesized at $1\,Al_2O_3$:$100\,SiO_2$:$15\,C_{22\text{-}6\text{-}6}(OH)_2$:$3\,H_2SO_4$:$6{,}000\,H_2O$, at 150 °C for 11 days, under sodium-free conditions. The hydroxide form of the surfactant was prepared through the anion exchange treatment of $C_{22\text{-}6\text{-}6}Br_2$. The conventional MFI zeolite (ZSM-5) used in this work was purchased from Zeolyst. All the zeolite samples possessed similar Si/Al ratios of 41–53. All catalytic reactions were carried out after converting zeolites into the H^+ form.

Full Methods and any associated references are available in the online version of the paper at www.nature.com/nature.

Received 16 February; accepted 13 July 2009.

1. Cundy, C. S. & Cox, P. A. The hydrothermal synthesis of zeolites: history and development from the earliest days to the present time. *Chem. Rev.* **103,** 663–701 (2003).
2. Corma, A. From microporous to mesoporous molecular sieve materials and their use in catalysis. *Chem. Rev.* **97,** 2373–2419 (1997).
3. Corma, A. State of the art and future challenges of zeolites as catalysts. *J. Catal.* **216,** 298–312 (2003).
4. Egeblad, K., Christensen, C. H., Kustova, M. & Christensen, C. H. Templating mesoporous zeolites. *Chem. Mater.* **20,** 946–960 (2008).
5. Tao, Y., Kanoh, H., Abrams, L. & Kaneko, K. Mesopore-modified zeolites: preparation, characterization, and applications. *Chem. Rev.* **106,** 896–910 (2006).
6. Tosheva, L. & Valtchev, V. P. Nanozeolites: synthesis, crystallization mechanism, and applications. *Chem. Mater.* **17,** 2494–2513 (2005).
7. Corma, A., Fornes, V., Pergher, S. B., Maesen, ThLM & Buglass, J. G. Delaminated zeolite precursors as selective acidic catalysts. *Nature* **396,** 353–356 (1998).
8. Corma, A., Fornés, V., Martínez-Triguero, J. & Pergher, S. B. Delaminated zeolites: combining the benefits of zeolites and mesoporous materials for catalytic uses. *J. Catal.* **186,** 57–63 (1999).
9. Corma, A., Diaz, U., Domine, M. E. & Fornés, V. New aluminosilicate and titanosilicate delaminated materials active for acid catalysis, and oxidation reactions using H_2O_2. *J. Am. Chem. Soc.* **122,** 2804–2809 (2000).
10. Holland, B. T., Abrams, L. & Stein, A. Dual templating of macroporous silicates with zeolitic microporous frameworks. *J. Am. Chem. Soc.* **121,** 4308–4309 (1999).
11. Jacobsen, C. J. H., Madsen, C., Houzvicka, J., Schmidt, I. & Carlsson, A. Mesoporous zeolite single crystals. *J. Am. Chem. Soc.* **122,** 7116–7117 (2000).
12. Tao, Y. S., Kanoh, H. & Kaneko, K. ZSM-5 monolith of uniform mesoporous channels. *J. Am. Chem. Soc.* **125,** 6044–6045 (2003).
13. Fan, W. *et al.* Hierarchical nanofabrication of microporous crystals with ordered mesoporosity. *Nature Mater.* **7,** 984–991 (2008).
14. Choi, M. *et al.* Amphiphilic organosilane-directed synthesis of crystalline zeolite with tunable mesoporosity. *Nature Mater.* **5,** 718–723 (2006).
15. Wang, H. & Pinnavaia, T. J. MFI zeolite with small and uniform intracrystal mesopores. *Angew. Chem. Int. Edn Engl.* **45,** 7603–7606 (2006).
16. Serrano, D. P., Aguado, J., Escola, J. M., Rodríguez, J. M. & Peral, Á. Hierarchical zeolites with enhanced textural and catalytic properties synthesized from organofunctionalized seeds. *Chem. Mater.* **18,** 2462–2464 (2006).
17. Xiao, F. S. *et al.* Catalytic properties of hierarchical mesoporous zeolites templated with a mixture of small organic ammonium salts and mesoscale cationic polymers. *Angew. Chem. Int. Edn Engl.* **45,** 3090–3093 (2006).
18. van Donk, S., Janssen, A. H., Bitter, J. H. & de Jong, K. P. Generation, characterization, and impact of mesopores in zeolite catalysts. *Catal. Rev.* **45,** 297–319 (2003).
19. Groen, J. C. *et al.* Creation of hollow zeolite architectures by controlled desilication of Al-zoned ZSM-5 crystals. *J. Am. Chem. Soc.* **127,** 10792–10793 (2005).
20. Groen, J. C. *et al.* Direct demonstration of enhanced diffusion in mesoporous ZSM-5 zeolite obtained via controlled desilication. *J. Am. Chem. Soc.* **129,** 355–360 (2007).
21. Gao, Y., Yoshitake, H., Wu, P. & Tatsumi, T. Controlled detitanation of ETS-10 materials through the post-synthetic treatment and their applications to the liquid-phase epoxidation of alkenes. *Micropor. Mesopor. Mater.* **70,** 93–101 (2004).
22. Pavel, C. C. & Schmidt, W. Generation of hierarchical pore systems in the titanosilicate ETS-10 by hydrogen peroxide treatment under microwave irradiation. *Chem. Commun.* **8,** 882–884 (2006).
23. Ryoo, R., Choi, M. & Na, K. Regularly stacked multilamellar and randomly arranged unilamellar zeolite nanosheets, and their analogue materials whose framework thickness were corresponding to one unit cell size or less than 10 unit cell size. Korean patent (applied, 2009).
24. Kresge, C. T., Leonowicz, M. E., Roth, W. J., Vartuli, J. C. & Beck, J. S. Ordered mesoporous molecular-sieves synthesized by a liquid-crystal template mechanism. *Nature* **359,** 710–712 (1992).
25. Beck, J. S. *et al.* Molecular or supramolecular templating: defining the role of surfactant chemistry in the formation of microporous and mesoporous molecular sieves. *Chem. Mater.* **6,** 1816–1821 (1994).
26. Shetti, V. N., Kim, J., Srivastava, R., Choi, M. & Ryoo, R. Assessment of the mesopore wall catalytic activities of MFI zeolite with mesoporous/microporous hierarchical structures. *J. Catal.* **254,** 296–303 (2008).
27. Bibby, D. M., Milestone, N. B., Patterson, J. E. & Aldridge, L. P. Coke formation in zeolite ZSM-5. *J. Catal.* **97,** 493–502 (1986).
28. Bibby, D. M., Howe, R. F. & McLellan, G. D. Coke formation in high-silica zeolites. *Appl. Catal. Gen.* **93,** 1–34 (1992).
29. Srivastava, R., Choi, M. & Ryoo, R. Mesoporous materials with zeolite framework: remarkable effect of the hierarchical structure for retardation of catalyst deactivation. *Chem. Commun.* **43,** 4489–4491 (2006).

Supplementary Information is linked to the online version of the paper at www.nature.com/nature.

Acknowledgements This work was mainly supported by the National Honor Scientist Program of the Ministry of Education, Science and Technology in Korea. Electron microscopic studies were performed with help from the measurement and analysis team at the National NanoFab Center, from the research supporting team at KAIST, and also at the Electron Microscopy Center (EMC) at Stockholm University with support from the Knut and Alice Wallenberg Foundation. Y.S. and O.T. thank the Swedish Research Council (VR) and the Japan Science and Technology Agency (JST), respectively.

Author Contributions R.R. initiated and managed the whole project, including the intuitive design of the structure-directing agents. M.C. and K.N. did synthesis and characterization (SEM, TEM, X-ray diffraction and adsorption). K.N. synthesized the multilamellar zeolite, and M.C. synthesized the unilamellar zeolite later. J.K. performed the catalytic testing. Y.S. and O.T. did high-resolution SEM and TEM investigations.

Author Information Reprints and permissions information is available at www.nature.com/reprints. Correspondence and requests for materials should be addressed to R.R. (rryoo@kaist.ac.kr).

METHODS

Synthesis of organic surfactant. $C_{22\text{-}6\text{-}6}Br_2$ was synthesized as follows: 39.0 g (0.100 mol) 1-bromodocosane (TCI) and 172 g (1.000 mol) *N*,*N*,*N*′,*N*′-tetramethyl-1,6-diaminohexane (Aldrich) were dissolved in 1,000 ml acetonitrile/toluene mixture (1:1 vol/vol) and heated at 70 °C for 10 h. After cooling to room temperature, the product was filtered, washed with diethyl ether, and dried in a vacuum oven at 50 °C. 56.2 g (0.100 mol) of the product and 24.6 g (0.200 mol) 1-bromohexane (Aldrich) were dissolved in 300 ml acetonitrile and refluxed for 10 h. After cooling to room temperature, the product was filtered, washed with diethyl ether, and dried in a vacuum oven at 50 °C.

Synthesis of nanosheet MFI zeolite. In a typical synthesis of multilamellar MFI nanosheets, tetraethylorthosilicate (TEOS, from TCI), $Al_2(SO_4)_3{\cdot}18H_2O$ (Aldrich), NaOH, $C_{22\text{-}6\text{-}6}Br_2$, H_2SO_4 and distilled water were mixed to obtain a gel composition of 30 Na_2O:1 Al_2O_3:100 SiO_2:10 $C_{22\text{-}6\text{-}6}Br_2$:18 H_2SO_4:4,000 H_2O. Water glass (an aqueous solution of sodium silicate, SiO_2/Na = 1.75, 29 wt% SiO_2) may be used as a silica source instead of TEOS. The resultant gel was transferred to a Teflon-coated stainless-steel autoclave, and heated at 150 °C for 5 days with the autoclave set to tumbling at 60 r.p.m. After crystallization, the zeolite product was filtered, washed with distilled water and dried at 120 °C. The product was calcined at 550 °C for 4 h under flowing air. For synthesis of unilamellar MFI, $C_{22\text{-}6\text{-}6}Br_2$ was converted to $C_{22\text{-}6\text{-}6}(OH)_2$ by passing aqueous solution through a column packed with anion exchange resin (MTO-Dowex SBR LCNG OH form, Supelco). The resultant solution contained 13 wt% $C_{22\text{-}6\text{-}6}(OH)_2$. The $C_{22\text{-}6\text{-}6}(OH)_2$ solution, TEOS, $Al_2(SO_4)_3{\cdot}18H_2O$ and distilled water were mixed to obtain a gel composition of 1 Al_2O_3:100 SiO_2:15 $C_{22\text{-}6\text{-}6}(OH)_2$:3 H_2SO_4:6,000 H_2O. The mixture was transferred to a Teflon-coated stainless-steel autoclave, and heated at 150 °C for 11 days with the autoclave set to tumbling at 60 r.p.m.

Characterization. X-ray diffraction patterns were taken with a Rigaku Multiflex diffractometer equipped with CuKα radiation (40 kV, 40 mA). SEM images were taken with a JEOL JSM-7401F at a low landing energy (0.3–0.6 keV, in gentle-beam mode). The samples were mounted without crashing and metal coating. TEM images were obtained with a JEOL JEM-3010 with accelerating voltage of 300 kV (Cs = 0.6 mm, point resolution 0.17 nm). N_2 adsorption isotherms were measured at the temperature of liquid nitrogen with an ASAP2020 volumetric adsorption analyser. The Brunauer–Emmett–Teller equation was used to calculate the apparent surface area from the adsorption data obtained at P/P_0 between 0.1 and 0.3. P, pressure; P_0, standard pressure.

Catalytic reactions. For catalytic reactions, all MFI zeolites synthesized in the present work were NH_4^+-ion exchanged with a 1 M NH_4NO_3 solution three times in all (NH_4NO_3/zeolite Al = 10, each time). The zeolite samples were converted to the H^+ form through calcination in air at 550 °C. An MFI zeolite sample in NH_4^+ form was purchased from Zeolyst (sample codes CBV 8014, Si/Al = 41). The zeolite was also calcined at 550 °C. This zeolite is referred to as conventional zeolite.

The catalytic reactions involving large molecules were carried out and analysed, following methods reported in the literature[26]. Cracking of branched polyethylene was performed in a Pyrex batch reactor equipped with an overhead stirrer. 10 g of polyethylene were placed in the reactor and melted at 350 °C. After the addition of 0.1 g of catalyst, the reactor temperature was further increased to 380 °C. During the reaction, N_2 gas was passed through the reactor at a rate of 40 ml min^{-1}. After 30 min reaction, the reaction yield was calculated from the mass change. Protection of benzaldehyde with pentaerythritol was carried out using a Pyrex batch reactor (EYELA chemistation) equipped with a reflux condenser. 1.06 g benzaldehyde (10 mmol), 0.68 g pentaerythritol (5 mmol), 4 ml toluene and 20 mg catalyst were placed into the Pyrex reactor and heated under stirring for 4 h at 120 °C. Condensation of 2-hydroxyacetophenone with benzaldehyde was carried out by heating a mixture containing benzaldehyde (0.75 g, 7 mmol), 2-hydroxyacetophenone (0.48 g, 3.5 mmol) and 50 mg catalyst at 150 °C for 14 h.

The methanol-to-gasoline reaction was performed at 400 °C in a fixed-bed Pyrex reactor (inner diameter, 13 mm) using 100 mg of catalyst. Before reaction, catalysts were activated at 550 °C for 2 h in a flowing air (30 ml min^{-1}). Methanol (99.6%) vapour was introduced by passing N_2 flow (50 ml min^{-1}) through a saturation evaporator at 30 °C (weight hourly space velocity = 11.0 h^{-1}). By considering oxygenates (methanol and dimethylether) as unconverted species, conversion was calculated by gas chromatography analysis. After prolonged reaction time, the used catalyst was collected and coke content was analysed by thermogravimetric analysis (TA Instrument). The coke formation inside micropores (internal coke) was calculated from a decrease in micropore volume (determined by N_2 adsorption), assuming coke density to be 1.22 g cm^{-3} (ref. 27). The coke content deposited on the external surface was calculated by subtracting the internal coke content from the total coke content.